HHS Public Access

Author manuscript

Acta Biomater. Author manuscript; available in PMC 2019 May 01.

Published in final edited form as:

Acta Biomater. 2013 August ; 9(8): 7977–7986. doi:10.1016/j.actbio.2013.04.040.

A mechanism for effective cell-seeding in rigid, microporous substrates

S. J. Polak,
1206 W. Green St, Urbana, IL 61801 USA, spolak2@illinois.edu

L. E. Rustom,
1206 W. Green St, Urbana, IL 61801 USA, rustom2@illinois.edu

G.M. Genin,
Department of Mechanical Engineering and Materials Science, and Department of Neurological Surgery, Washington University School of Medicine, St. Louis, MO 60613 USA, genin@wustl.edu

Michael Talcott, DVM, DACLAM, and
Division of Comparative Medicine, Washington University School of Medicine, 660 S. Euclid Ave. Box 8061, St. Louis, MO 60613 USA, mtalcott@wustl.edu

A. J. Wagoner Johnson
1206 W. Green St, Urbana, IL 61801 USA, ajwj@illinois.edu

Abstract

Seeding cells into porous ceramic substrates has been shown to improve outcomes in surgical repair of large bone defects, but the physics underlying cellular ingress into such scaffolds remains elusive. This paper demonstrates capillary forces as a novel, yet simple, self-loading or self-seeding mechanism for rigid, microporous substrates. Capillary forces drew cells through a microporous network with interconnections smaller than the diameter of the cells in suspension. Work here emphasizes CaP-based bone scaffolds containing both macroporosity (>100μm) and microporosity (5–50μm), as these have been shown to improve bone formation *in vivo* as compared to their macroporous counterparts. We hypothesize that capillary force driven self-seeding in both macro and micropores may underlie this improvement, and present a mathematical model and experiments that support this hypothesis. The cell localization and penetration depth within these 2D substrates *in vitro* depended upon both the cell type (size and stiffness) and the capillary forces in the microstructure. Additional experiments showing that cell penetration depth *in vitro* depends on cell size and stiffness suggest that microporosity could be tailored to optimize cell infiltration in a cell-specific way. Cells are also drawn into the microporous network *in vivo*. Results have important implications for design of scaffolds for the healing of large bone defects, and for controlled release of drugs *in vivo*.

Keywords

bone; porosity; cell seeding; scaffold; microstructure

1 Introduction

Bone defects beyond a critical size do not heal spontaneously and, in some cases, repair and healing do not occur even with the use of allografts or autografts. Repair approaches using engineered scaffolds combined with soluble growth factors such as recombinant human bone morphogenetic protein (rhBMP-2) or stem-cell therapy have been largely unsuccessful or have resulted in severe clinical side effects [1,2]. Efficacy of engineered scaffolds has been shown to be enhanced by pre-seeding with autologous bone marrow [3]. Because cell migration to a wound site can take days [4,5], which delays vascularization and tissue formation, commercial products exist that increase the degree of cell seeding[6]. For example, the chronOS system (Synthes Biomaterials, Oberdorf, Germany) uses a scaffold in a vacuum-sealed bag with the aim of enhancing the penetration of bone marrow cells into the scaffold. However, the physics underlying successful infiltration of cells into a ceramic scaffold is not yet known, and guidelines for optimization of products of this character are not yet available.

This paper tests the hypothesis that capillary forces play a central role in seeding of microporous substrates. The goal is to demonstrate a multi-scale, self-loading mechanism that may be tuned to selectively incorporate cells into a rigid scaffold. While this mechanism is quite general, we are specifically interested in the self-seeding of calcium phosphate (CaP)-based bone scaffolds containing both macroporosity (>100 μm) and microporosity (5–50 μm), or “multiscale porosity.” CaP-based material systems are favored for interfacing with bone because they are biocompatible, osteoconductive, and have composition similar to the mineral phase in bone [4]. The system tested in this paper is unique among CaP-based systems in two ways. First, we precisely control porosity on two distinct length scales. We fabricate scaffolds using a robotically controlled, directed deposition, ink extrusion system [7–10], which allows us to control macropore size and geometry directly. We control microporosity in part by incorporating different ink formulations in a single scaffold [7] and/or through the use of PMMA microspheres as sacrificial porogens. Whereas others control microporosity primarily through sintering or through use of foaming agents [5,11], use of the PMMA microspheres generates uniform micropores and allows us to vary micropore size and fraction through ink formulation and bead characteristics [12].

Microporosity, in addition to the requisite macroporosity [5,13],' has been shown recently to enhance bone regeneration in CaP-based scaffolds [5,11,13–15]. Cells populate micropores within scaffold rods and produce bone both in the micropores and the macropores of scaffolds containing multiscale porosity [15,16]. Scaffolds with microporous (MP) rods and implanted *in vivo* displayed a larger volume fraction of bone, bone that was more uniformly distributed, and a shorter healing time when compared to non-microporous (NMP) scaffolds, or scaffolds with solid rods[14]. Multivariate statistical analysis suggests that microporosity affects bone regeneration more strongly than the potent osteogenic growth factor, BMP-2[14].

While there is general agreement that microporosity is beneficial, there is little understanding of the mechanisms governing bone growth in the presence of microporosity and therefore no definitive design rules to guide basic research or translation to the clinic.

Candidates include stimulation of cells by surface roughness, protein attachment, and precipitation of biological apatite, all of which are enhanced with increased surface area in the presence of microporosity [11,17–19]. With so many, often interconnected variables, the barriers to understanding the role of microporosity are significant. This work seeks to clarify this role through study of a well-defined system.

The work presented here suggests a tunable self-loading or self-seeding mechanism and describes the basic physics of the process. This mechanism could alter the *in vivo* response to microporous CaP scaffolds. We hypothesize that it could also potentially explain the enhanced bone regeneration in macropores observed by us for our scaffold system [14,16,20] and by others independently [5,9,11,21]. We first develop a model of capillary pressure generated by a specific microstructure of interest, and validate the model using capillary rise experiments. We then calculate the theoretical critical pressure for several types of cells to enter a rigid capillary and compare this to the capillary pressure generated by the microstructure. The results presented support the hypothesis that capillary forces will not only localize cells to the substrate surface, but will also deform them, squeezing them through the micropores and interconnections and leading to an effective self-seeding of the micropores. We find through additional experiments that cell penetration depth into the microporous network *in vitro* is cell type-dependent and that the measured depths correlate with published cell cortical tension and size. In addition to the *in vitro* experiments that highlight the physics of the self-seeding, we demonstrate that this seeding also occurs upon implantation of scaffolds into a bone defect *in vivo*. Finally, we show that small, non-deformable particles penetrate deep into the microstructure, indicating that capillary forces could also be used to sequester particles to micropores as a novel mechanism for controlled drug delivery.

2 Materials and Methods

2.1 Substrate fabrication: scaffolds for *in vivo* experiments, 2D substrates for *in vitro* experiments

Scaffolds and substrates were fabricated using the CaP (hydroxyapatite) ink preparation method and direct deposition system described previously [8,10,12,14,15]. The scaffolds that were used in the *in vivo* experiments here (see Section 2.5 details of the in vivo study) had the same pore size distribution as in our previous work, 4.86 ± 3.62μm, nominally 5μm [12,14–16]. CaP powder (Riedel-de-Haen, Seelze, Germany) was calcined at 1100°C for 10 hours, then ball-milled in 100% ethanol for 14 hours and then dried at 125°C for 15 hours. This process broke up aggregated particles and improved the uniformity of the particles. Chemical additives were incorporated into the CaP to generate a slurry for extrusion by the deposition system. Poly-methyl methacrylate (PMMA) microspheres (Matsumoto Microsphere M-100, Tomen America, New York, NY) were added to serve as sacrificial porogens in the CaP slurry that was used to deposit microporous (MP) scaffolds. The post-deposition sintering burned out all additives including the PMMA microspheres.

Brick-shaped lattices made of alternating layers of orthogonal rods, later machined into cylindrical scaffolds, and the 2D substrates were fabricated with the directed deposition system using a 0.51mm and 0.61mm nozzle tip (EFD), respectively. Samples were deposited

under lamp oil and remained in the oil for 12 hours after deposition to set. The oil was drained and the lattices dried for another 12 hours. All scaffolds and substrates were sintered for 2 hours at 1300°C, with a slow ramp to temperature over several hours and a similar ramp for cooling [12,14–16,20,22–24]. The organic additives in the ink and the PMMA microspheres burned out at approximately 900°C. The resulting pores were the focus of our study and were dominant over the ≤1 micron pores associated with sintering. The latter were present in both microporous and non-microporous samples, but were not interconnected.

The brick-shaped lattices were vacuum-embedded in wax and then machined into two, 5 mm diameter and 8 mm height cylindrical scaffolds using an end-mill. The machining wax was burned out by heating samples to 525°C for 1 hour. The scaffolds were sterilized by autoclave prior to implantation. Surgical procedures are described in Section 2.5.

2.2 Model of the microporous microstructure, capillary forces, and cellular ingress

Model for dependence of capillary pressure on microstructure—We developed a model of the microstructure and verified the model experimentally in order to establish the influence of microstructure on the capillary forces that draw cells into the micropores. The model predicts capillary force, F_C, exerted on cells by a scaffold as a function of intrinsic material parameters (contact angle of the solid/fluid/air interface, α, and surface tension of the fluid, σ) and an experimentally controllable microstructural parameter (the wetted perimeter of a capillary tube, P_W):

$$F_c = P_w \sigma \cos(\alpha) \quad (1)$$

For a cylindrical tube of radius r the wetted perimeter is $P_w = 2\pi r$. However, for a microporous scaffold the wetted perimeter must be estimated via statistical methods.

To estimate the wetted perimeter we performed Monte Carlo simulations using a custom code written in the Matlab environment (MathWorks, Natick, MA). The code modeled a population of micropores using a set of rigid, non-overlapping spheres, with radii following a normal distribution of prescribed mean and standard deviation. The mean and standard deviation that were used were measured experimentally from the same system as part of another study [12]. Micropores were distributed randomly in rectangular volumes of height 10μm and prescribed square cross-sectional area A to achieve a prescribed void fraction, ε.

Statistical analysis of the wetted perimeter per unit area was conducted on ten representative two-dimensional cross-sections of each volume, taken at one-micron increments through the ten micron height (see Figure 2). Summing the perimeter of all the circles created by sectioning the spheres gives the total wetted perimeter of each section. Because there is a distribution of pores in the microstructure, and therefore spheres in the model, an average wetted perimeter comes from the ten sections. The cross-sectional area A was varied to ensure a sufficiently large sampling volume and the existence of the expected linear relationship between P_w and A:

$$P_w = C\varepsilon A \quad (2)$$

where the constant of proportionality C is a function of the mean and standard deviation of the void radius. Thus, the total capillary force per unit cross-sectional area for a specific microstructure is:

$$F_c = C\varepsilon A\sigma\cos(\alpha) \quad (3)$$

This force can be converted to a mean capillary pressure, $\overline{P}$, associated with capillaries in a specific microstructure by dividing by the mean cross-sectional area of voids within a cross-section, which by Delesse's principle is εA [25]:

$$\overline{P} = C\sigma\cos(\alpha) \quad (4)$$

The mean capillary pressure is then a function of the geometrical parameter C and the two material parameters σ and α. Note that this drops to zero for a scaffold that is already filled with fluid, because the parameters are a property of the air/fluid/solid interface.

Two microstructures were simulated using the Matlab© program in order to determine their respective wetted perimeter and resulting capillary pressure generated. The pore size distributions were determined in previous work [12], using Mercury Intrusion Porosimetry (MIP). These were 4.86 ± 3.62μm, nominally 5μm, and 9.6 ± 6.68μm, nominally 10μm, diameter pores. The measured pore size distributions account for sintering pores, which are on the order of <1μm, the pores generated by the sacrificial porogens used in the CaP ink, which are on the order of 5μm [12], and the interconnections between pores, which are on the order of 2μm. Because the algorithm takes into account the pore size distribution in a specific microporous network, it can be applied to any porous microstructure with known pore size distribution.

Model validation—To validate the model, we experimentally measured the pressure drop, ΔP, across two substrates with the different microstructures used in the model, using capillary rise tests and the relation:

$$\Delta P = \rho g \Delta h \quad (5)$$

Then, we implemented the measured pressure in Equation 3 to determine the contact angle that would be required to generate that pressure. Because the material and fluid system are the same, and only the microstructures are different, we would expect the contact angle to be the same.

For the rise tests, 2D MP substrates with dimensions 3×4×45mm were suspended above a beaker of water and then brought in contact with the water. The height of the water, Δh, was recorded at regular time intervals as it rose through the sample. This was repeated for five samples for each microstructure. The maximum height for the substrates with 5μm pores was greater than the height of the substrate itself, therefore the maximum height was determined by fitting an equation to the height versus time curve and using the asymptomatic value as the maximum height. Finally, we compared the calculated contact angle to the measured contact angle for a solid, non-porous substrate using a Canon© EOS-5D Mark II SLR digital camera. We also compared the pressures determined from the capillary rise experiments to the pressures calculated from the simulation for further validation.

Modeling of cellular ingress—The effect of cell size and stiffness on cellular ingress was assessed by comparing the microstructure-dependent mean capillary pressure $\overline{P}$ from Equation 4 to the pressure P_{crit} needed to draw a cell of a certain size and stiffness into a capillary tube. The first question to ask is what stiffness to use given that cellular stiffness varies over many orders of magnitude from tens of Pascals for laser tracking microrheology [26] to tens of kPa for nanoindentation [26–27] to nearly a MPa for activated cells in a 3D tissue construct [29–31]. For the case of cells entering capillary tubes, the stiffness is likely no longer dominated by cytoskeletal proteins that disassemble under high strain (cf. [33–34]) but rather by cortical tension. Following work on micropipette aspiration of cells, the critical pressure depends on the pore radius, R_{p}, cell radius, R_{c}, and the cortical tension of the cell, γ_{ten}, which is a measure of cell stiffness [26–34]

$$P_{crit} = 2\gamma_{ten}\left(\frac{1}{R_p} - \frac{1}{R_c}\right) \quad (6)$$

The average pore radius from the *in vivo* study, 2.5μm, was used for R_{p} in the results from the calculations, which are summarized in Table 1.

2.3 Cell localization *in vitro*

In order to determine the effect of capillary forces on cell localization to a substrate surface, we seeded cells *in vitro* on the top of 2D substrates in the presence and absence of capillary forces and then measured the cell density. To isolate the effect of capillary forces, we used two types of substrates, non-microporous (NMP, Figure 1b) and MP (Figure 1c), and two different initial conditions, PBS-submerged and dry. Of these, only the dry MP substrates could generate capillary forces. Submerging the substrates for approximately 30 seconds, thus filling the pores with PBS, eliminated capillary forces, but still maintained other surface properties such as surface roughness, pore size, and pore fraction. Comparing MP and NMP substrates separated the effect of the microstructure from the wet or dry surface.

The substrates were homogeneous CaP (hydroxyapatite) disks 0.74mm in height made with MP or NMP CaP or they were composite 1.31mm in height with one hemi-circle MP CaP and the other hemi-circle NMP CaP. Substrates were either seeded with cells dry or after

submersion in PBS to fill the micropores. Care was taken to ensure that procedures were performed quickly to avoid any effects of reprecipitation. Although these effects are large in thin specimens of biological hydroxyapatite (e.g. [26]), they are sufficiently small in larger geological hydroxyapatite specimens that little reprecipitation was expected in our study (cf. [6]). The four treatments were: MP dry, MP wet, NMP dry, and NMP wet.

Cells from a murine pre-osteoblastic cell line (D1s) were prepared by staining with CellTracker™ Green CMFDA (Invitrogen, Grand Island, NY) and seeded on the substrates at a concentration of 3×10^5 cells/ml. The cells were allowed 15 minutes to adhere before rinsing and imaging with a fluorescent microscope (Zeiss Axiovert 200M, Beckman ITG). Cells in five randomly selected regions on each two-dimensional substrate were counted to determine a cell density for each substrate.

2.4 Cell and polystyrene bead penetration *in vitro*

Penetration of three cell types into a microporous substrate was measured *in vitro*: a murine osteoblast cell line MC-3T3-E1 subclone 4 cells (E1), D1s that were used in the cell localization experiments, and primary rat MSCs. All cells were tagged with CellTracker™ Green CMFDA (Invitrogen, Grand Island, NY) and resuspended to a concentration of 5×10^5 cells/ml. The MP substrates used in these experiments were 10×20×0.3mm sheets, approximately the size of a microscope slide, with a void fraction of 0.46 and a pore diameter of 4.86 ± 3.62μm [12]. A microscope slide was affixed to the bottom of a 10cm diameter petri dish and then 20μl of the diluted bead solution was pipetted along the edge of the top of the slide. The MP substrate was brought into contact with the edge of the slide, bringing the substrate and the cell solution in contact (see Figure 4a). This lasted approximately 5 minutes, until all of the solution was absorbed into the substrate and the fluid ceased to move through the micropores. Substrates were imaged with a fluorescent microscope and the penetration distance measured. To explore self-loading for drug delivery applications, the same experiment was repeated using a 1% w/v stock solution of SPHERO™ high intensity fluorescent beads (Spherotech, Crystal Lake, IL) with a diameter of 1.84 μm, diluted 1:20 with DI water, instead of a cell suspension.

2.5 Surgical procedure

Four-five month old, 60 kg male Yorkshire-cross pigs were used for the in vivo experiments in this study. All animal experiments were done in accordance with the Guide for the Care and Use of Laboratory Animals (8th Ed.) and approved by the Washington University Animal Studies Committee. Pigs were fasted for approximately 12–14 hours prior to surgery and were sedated using a cocktail of Telazol (4 mg/kg), ketamine (2 mg/kg) and xylazine (2 mg/kg) IM. Anesthesia was maintained using isoflurane gas (1–5%) following endotracheal intubation, and vital signs were monitored throughout the procedure. Bilateral retromandibular incisions were made through the skin and subcutaneous tissue, avoiding the facial nerve, artery and vein. At the inferior boarder of the mandible the periosteum was cut and reflected to expose the bone. A Dremel rotary drill (Robert Bosch Tool Corp, Racine, WI) with a trephine bur was used to create three 5 mm diameter bicortical defects on the lateral surface at the angle of each of the mandibles. The 5 mm diameter holes extended through the thickness of the ramus. Constant irrigation with saline at the osteotomy site was

required to maintain the integrity of the tissue. Animals were implanted with 5mm diameter MP scaffolds that were either dry or that had been submerged in saline prior to implantation. The scaffolds submerged in saline were tapped against the container wall to ensure all the trapped air had escaped the scaffold. Each hemi-mandible had three defects created for a total of six defects per animal. Scaffolds were press-fit into the defects and remained in the animal for 30 minutes before removal; no differences were observed in additional experiments for which the scaffolds were implanted for 15 minutes or 60 minutes before removal.

2.6 Histology

Scaffolds removed from the animals after 30 minutes were immediately placed in 10% formalin. After 12–24 hours the samples were dehydrated in increasing concentrations of ethanol in DI water before PMMA embedding. Histological procedures are similar to those reported previously [16]. Briefly, on day one of embedding, the samples were placed under vacuum in a 1:1 mixture of methyl methacrylate (MMA) monomer (Acros 127140010) and ethanol. On day two, the samples remained under vacuum and were placed in a 100g MMA per 1g benzoyl peroxide (Aldrich 17,998–1) mixture. On day three, the samples remained under vacuum in a 100g MMA per 1g benzoyl peroxide per 20g PMMA (Acros 41806–0010) mixture. After 24 hours, the samples were moved to a 25°C water bath. The temperature was increased by ~1°C per day until the samples polymerized. Upon polymerization the samples were cured at 60°C for 1 hour.

Samples were then removed from their containers and affixed to wooden dowel rods prior to diamond saw sectioning. Sections were cut approximately 1.2mm thick and mounted onto acrylic slides. The slides were polished using a series of sand paper grits down to <200μm in thickness. Samples were then stained with Sanderson's rapid bone stain and imaged using light microscopy (AxioImager A1, Ziess, Inc.).

3 Results

3.1 Characteristics of the HA substrates and scaffold system

The scaffold system is one used in previous work [14–16,20]. Briefly, scaffolds consist of layers of orthogonal rods of HA, approximately 395μm in diameter (Figure 1). The center-to-center spacing of the rods is 753μm in-plane and 646μm out-of-plane. The rods themselves are either solid (Figure 1b) or microporous (Figure 1c). In previous work cylindrical scaffolds were implanted in the mandibles of pigs for times ranging from 3 to 24 weeks. Microporous samples contained bone and cells within the micropores (Figure 1d). The 2D substrates used consisted of slabs made from the same inks.

3.2 Model predicts capillary forces in a microporous network

We developed a model of the microstructure and verified the model experimentally in order to estimate capillary forces in the microporous network in scaffolds used in our previous *in vivo* studies (Figure 1) [14–16,20] as well as for other microstructures of interest. The model, described in Section 2.2, relates contact angle, surface tension, surface area, and microstructure to the capillary pressure generated by the microstructure.

One of the microstructures modeled was used in previous studies [14–16,20] and had nominally 5μm diameter pores (Figure 1c). The other had a different pore size distribution of 9.6 ± 6.68μm diameter pores [12], or nominally 10 μm diameter pores. Both substrates had a void fraction of 0.46. The constant, C, determined by the model and which relates the wetted perimeter to the void area for a given microstructure according to Equations 2–4, was $0.68\mu m^{-1}$ and $0.40\mu m^{-1}$, for the respective microstructures. The contact angle measured as described in Section 2.2 was an average of five samples, 89.8 ± 5.0°. Using the surface tension for water as 0.072N/m [27] and the measured contact angle along with Equation 3, the calculated simulated pressures in the substrates with the smaller and larger micropores were 584Pa and 345Pa, respectively.

For the capillary rise tests, the maximum heights of the liquid in the substrates with nominally 5μm and 10μm diameter pores were 60mm (R^2=0.95) and 42mm (R^2 = 0.96), respectively. Using the equation for hydrostatic pressure (Equation 5), the resulting measured pressures in the substrates were 588Pa for the 5μm diameter micropore samples and 412Pa for the 10μm diameter micropore samples. The corresponding contact angles required to achieve these pressures were 89.3° and 89.2°, respectively. Equivalent contact angles were expected given that contact angle is a property of the material and fluid. These results helped to further validate the model of the microstructure.

3.3 Capillary pressure in the microporous substrates exceeds the theoretical critical pressure to draw in cell types relevant to bone formation

With values for pressure generated by the microstructure of interest, we next calculated the critical pressure, P_{crit}, required for a single cell to deform and enter a capillary tube *in vitro* using Equation 6 [28] and data in the literature [29–37] for several cell types (Table 1). The critical pressure was compared to the pressure generated based on the model of the microstructure, in order to predict whether the pressure is sufficient to draw cells into the microporous network.

With the measured capillary pressure in the scaffold rods of 588Pa, the microstructure in Figure 1c would generate large enough capillary forces to draw in neutrophils, osteoblasts, E1s, and MSCs. The calculated critical pressure was lowest for neutrophils, at 7.77Pa, because they have both a small radius, 4.2 μm [18], and small cortical tension, 2.4×10^{-5} kg/s^2 [29] On the other hand chondrocytes had the highest critical pressure at 1131Pa, largely due to their high cortical tension [30,32]. An important point from this result is that there is a large range of critical pressures to draw different types of cells into the microporous network and a range of pressures can be generated for different microstructures. This suggests that the microstructure could potentially be tailored to select specific cell types.

3.4 Cells localize to microporous substrate surface in the presence of capillary forces *in vitro*

To study cell localization *in vitro*, cell suspensions were placed on the surface of wet (PBS-submerged) and dry, MP and NMP substrates and cell density measured. Significantly more cells localized to the dry MP substrates, the only substrates with active capillary forces, as

compared to both the PBS-submerged substrates, whose pores were filled with fluid, and the dry NMP substrates (Figure 3a,b). Cell density was five times greater on dry MP substrates as compared to dry NMP substrates, and eleven times greater than on PBS-submerged MP substrates (Figure 3d). The differences seen between the other treatments groups were not statistically significant but may be due to the presence of small sintering pores. The stark contrast is apparent in a dry-treatment composite substrate that shows a distinct boarder between the MP and NMP domains (Figure 3e–i). As the presence of capillary forces was the only difference for the dry MP, we attributed the cell localization to these forces.

3.5 Capillary forces draw cells into microporous network *in vitro* with cell-type depth dependence

Next, we investigated *in vitro* whether capillary force, or pressure, generated by the microstructure was sufficient to deform the cells and draw them into micropores and, if so, if the cell penetration depth was cell-type dependent. We designed and conducted experiments to constrain the cells to travel primarily in one direction. This allowed us to measure the linear distance traveled by the cells, which was not possible with the surface localization experiments.

The cell penetration depth into the microporous network *in vitro* depended on the cell type (Figure 4b–d). E1 cells traveled furthest at 165.6 ± 7.8μm (± standard error) and this was significantly different than the other two cell types. MSCs and D1s penetrated 116.1 ± 5.2μm and 88.2 ± 6.8μm, respectively (Figure 4f), but there was no statistical difference between them. Importantly, these depths are of similar magnitude as the radius of the scaffold rods in scaffolds used in the *in vivo* study (Figure 1) [14–16]. The results from these experiments clearly demonstrate that capillary forces generated by a microporous network will draw a range of cell types into the network and that the final depth is cell-type dependent.

3.6 Capillary forces as a potential self-loading mechanism for protein and drug delivery

We propose that self-loading via capillary forces and then release *in vivo* could be an effective protein and drug delivery mechanism. To demonstrate the self-loading potential, we repeated the capillary rise tests *in vitro* using non-deformable, fluorescent, polysterene beads – 1.84 μm in diameter. The bead suspension wicked into the microporous network and penetrated 2.05±0.07mm (Figure 4e) into the 10mm long substrate. The fluid, however, traveled the entire 10mm. The relatively large bead penetration distance, as compared to cells (Figure 4), suggests that drugs tethered to or encapsulated by small, non-deformable particles can also be drawn into a microporous tissue scaffold via capillary forces. Proteins or drugs in solution would penetrate even further because their weight and size would be a fraction of those of the polymer beads.

The penetration of the cells described in Section 3.5 shows that larger, deformable drug carriers, such as gelatin microspheres, could also be drawn in. This micropore-generated capillary pressure provides a “self-loading” mechanism for endogenous proteins or exogenous proteins and drugs relevant to bone formation at the time of implantation or prior to implantation, respectively. The initial sequestration by capillary forces would mitigate a

bolus delivery and the diffusion through the microporous network could provide a steady release. The release rate may be tailored by modifying the microstructure to facilitate or hinder diffusion.

3.7 Capillary forces enable self-seeding of micropores *in vivo*

The *in vitro* experiments conducted in this study clearly show that capillary forces localize cells to the substrate surface and that cell penetration into the microporous network is cell-type dependent. However, the environment *in vivo* is more complex and heterogeneous. Further, clotting may influence the seeding. Therefore we implanted scaffolds into a bone defect *in vivo* in order to demonstrate that cells are drawn into micropores *in vivo* as well, and that this process is also dependent on capillary forces. Capillary forces were eliminated in some MP scaffolds in the same manner they were for the *in vitro* studies; some MP scaffolds were submerged in PBS to fill micropores with fluid.

Results show that the endogenous cells are, in fact, drawn into the microporous network via capillary forces. Cells penetrated the scaffold rods approximately 100μm, consistent with what was observed in cell penetrations experiments in 2D substrates *in vitro* for all three cell types (cf. Figure 4). This distance is also the same size scale as individual trabeculae in trabecular bone. Cells were not present in rods that had fluid-filled micropores upon implantation (Figure 5). Cells were not present in the outer edge of scaffold rods where the scaffold had been machined from its lattice either (Figure 6a and b). SEM images reveal that the micropores at the machined interface are filled with debris (Figure 6c). This both provides an explanation for the lack of cell penetration and strengthens the argument that capillary forces are important to cell penetration.

4 Discussion

4.1 Model predicts capillary forces for microporous network

The model we developed and validated allows us to predict the capillary forces generated in a microporous network. Combined with the estimation of the critical pressure for a cell to enter a single pore, the model demonstrates that certain microstructures could potentially draw in cells via capillary force alone. This model could be used to design microstructures that allow certain cells to enter immediately upon implantation, while preventing others from entering. Scaffolds could also be designed and fabricated with distinct domains [7] that would generate different capillary pressures at specific locations within the scaffold. This could potentially improve bone regeneration over larger distances than were previously thought possible. While we focused on the microstructure used in our previous work, the simple model could be used to calculate capillary forces generated for a wide range of porous networks.

4.2 Capillary forces for cell localization

A critical step for bone regeneration within a scaffold *in vivo* is for the relevant cells to simply reach the surface of the scaffold material, throughout the 3D scaffold structure and deep into the defect. In fact, this may be the limiting step in healing of large defects. Even for small defects, the distance cells must travel relative to their size is significant. Cells may

reach the scaffold surface by migration from the defect periphery, but this mechanism alone may prolong regeneration and/or result in incomplete healing, depending on the size of the defect. *In vivo*, this cell localization by capillary forces could draw cells to the surface of the scaffold rods, drawing in cells relevant to bone formation deep within the scaffold, seeding the macropores, and removing the dependence on cell migration to the surface for bone regeneration. Thus, importantly, the cell localization mechanism could be effective even in the event that micropores were too small for cells to enter. This mechanism could lead to faster healing and the ability to heal larger defects than was previously possible.

To isolate the effects of capillary forces on cell localization, we seeded cells on substrates in vitro with identical microporous networks, but different capillary forces. The wet MP substrate was identical to the dry MP substrate except that the micropores in the wet substrates were filled with PBS prior to seeding the cells. As empty micropores were essential to generating capillary forces, the wet MP substrate had significantly fewer cells on the surface as compared to the dry MP substrate (Figures 3 and 5). By comparing the wet and dry NMP substrates *in vitro* we demonstrated that the PBS on the substrate surface did not alter the cell localization. Demonstration of increased cell localization to the surface of dry MP substrates illustrates an important effect of capillary forces. The 11-fold higher cell density on the surface of the dry MP substrate (Figure 3) compared to the wet MP substrate, shows that capillary forces can be used to localize the patient's cells on a scaffold either prior to implantation into the defect or actually as the scaffold is placed directly into the defect site. As attracting the cells is an important first step in bone formation and healing, this suggests that documented increase in bone volume seen in MP over NMP scaffolds [5,11,14,19,20] *in vivo* may be partially due to this initial localization of cells.

4.3 Capillary forces draw cells into the microporous network both *in vitro* and *in vivo*

In addition to increasing cell localization, MP substrates and scaffolds showed cell penetration into the microporous network both *in vitro* (Figure 4) and *in vivo* soon after implantation (Figure 5 and 6), respectively, but only in the presence of capillary forces. The *in vitro* experiments showed this to be true for a range of cell types, including cells relevant to bone formation such as E1s (osteoblasts), MSCs, and D1s (pre-osteoblasts) (Figure 4b–d). Furthermore, the final penetration depth was cell-type dependent.

The measured *in vitro* cell penetration depths were consistent with the critical pressure calculations (Table 1, Equation 6). If the calculated critical pressure for the cell to enter a pore is lower, we expect cell penetration into the network to be easier and therefore the cell would travel further. Recall the critical pressure depends on both the cell radius and cortical tension according to Equation 6. The critical pressure for E1s was lower than that of MSCs, at 265Pa versus 320Pa, respectively (Table 1), thus we expect the E1s to travel further, and they did. E1s had a similar radius in suspension compared to D1s (Figure 4g, h) and both cell types were smaller than MSCs (Table 1). We speculate that the difference in penetration depth between E1s and D1s may therefore be due to a difference in cortical tension. The lower cortical tension would allow E1s to deform more easily and therefore travel further in the microporous network. Finally, the difference in penetration depths measured for these

cell types suggests that the microstructures could be tailored to select specific cells to penetrate the microporous network *in vivo*.

To our knowledge, in the majority of other work on CaP scaffolds control of microporosity is through sintering time and temperature [5,11,21]. Using this approach, the change in size and fraction of micropores is limited and the micropores are a smaller fraction of the size of the cells. These scaffolds may allow for cell localization, but not cell penetration. The fabrication process we use allows us to incorporate sacrificial polymer microspheres of different sizes and in different fractions, which burn out during sintering [8,10]. Our approach allows us a much broader range and more control of pore size and fraction [12] and therefore capillary pressure generated by the microstructure.

While the cell's critical pressure and the capillary force generated by the microstructure can be used to determine if a cell will enter the microporous network, they cannot be used to determine how far a cell will penetrate. The frictional losses that result from a cell deforming through a small pore or pore interconnection limit the cell penetration distance. However, the calculations from the model and the critical pressure do indicate whether a cell will enter the microstructure and can help predict how far one cell type will penetrate compared to another. Additional experiments and modeling may allow us to quantitatively predict the frictional losses associated with cell deformation through pores.

Data from these experiments and model present capillary forces as a tunable mechanism for localizing cells within macropores of these rigid CaP scaffolds as well as for cell-seeding in micropores. While results clearly show that the cell penetration occurs *in vivo*, results do not explicitly show that the presence of cells in micropores enhances bone regeneration macropores. This remains to be proven and work is underway. We further recognize that the cell population within micropores in our previous work [refs] at 3, 6, 12, and 24 weeks *in vivo* could include daughter cells from those that entered via capillary forces or cells that migrated into the microporous network. Evidence of cell migration contributing to the cell population in micropores is in previous work [ref]. There BMP-2 was added to gelatin microspheres, which were then suspended in a dilute gelatin solution. This solution was added to dry scaffolds and implanted in the pig ramus for up to 24 weeks. Scaffolds with BMP-2 so administered also contained cells in micropores. However, the bone in the macropores did not differ between scaffolds with or without BMP-2 [ref]. We concluded that capillary forces drew BMP-2 into micropores and that the presence of the BMP-2 in those micropores may have been a strong enough driving force for cells to migrate, proliferate, differentiate, and form bone in the micropores. This does support our hypothesis that the capillary-force induced cell localization contributes to enhanced bone regeneration.

4.4 Capillary forces as a potential self-loading mechanism for protein and drug delivery

The entrance of cells into the microporous network demonstrates that proteins, which are substantially smaller than cells, or other carriers will enter as well. We postulate that capillary forces generated by the microporosity can be used as a self-loading mechanism for drug delivery, with or without a carrier. Our experiments showed that non-deformable beads with diameters smaller than the average pore traveled the furthest in through the microstructure, approximately 2mm (Figure 4e). The molecules inside or coating the carrier

could diffuse out over time without a significant bolus effect and have a chemotactic effect on cells within the scaffold macropores. Coupled with the evidence showing that the microstructure localizes cells to the surface, this creates an effective system where cells are drawn to the surface and drugs are released over time to, for example, promote differentiation or migration.

5 Conclusion

Taken together, the results presented show that capillary forces can play a central role in seeding microporous substrates. We suggest this as a novel, yet simple, mechanism that could potentially account for the presence of cells and bone in micropores in CaP-based bone scaffolds [15,16]. This work clearly demonstrates that capillary forces can play an active role in cell localization to the surface of a microporous CaP substrate (Figure 3). We also definitively show, both *in vitro* and *in vivo*, that these forces are capable of deforming the cells and drawing them into the microporous network (Figures 3, 4 and 5). We hypothesize that these two processes, cell localization to the surface of the material deep within the scaffold macropores as well as cell sequestration or entrapment in micropores, may be responsible for the results in the literature and from our lab showing enhanced bone regeneration in the presence of scaffolds containing both macro and microporosity [5,9,11,14–16,19]. In our work this enhancement was equal to or better than BMP-2 by some measures. We further hypothesize that the cell localization and penetration could result in the multiscale osteointegration that we reported previously [15,16]. We emphasize that this study does not prove this hypothesis, further work is necessary, nor does it consider other relevant factors such as proteins and cell adhesion [38].

This study marks the first identification of a governing principle potentially underlying observations of the efficacy of micropores, and predictions match observations well. Results from the simulations and experiments will allow scaffolds to be designed with appropriate microstructures to self-load with cells and proteins, potentially enhancing healing and improving scaffold/tissue integration. Microstructure could be tailored to select or draw in specific cells to a certain depth, or for controlled drug release: given that different types of cells penetrate different distances into the 2D substrates (cf. Figure 4), the possibility of microstructural features could be optimized for particular cell types. Results from this study have important implications in bone scaffold design and the potential for healing of large bone defects.

Acknowledgements

Fellowship assistance was awarded to S.J.P. by the University of Illinois at Urbana-Champaign (UIUC) College of Engineering Roy J. Carver Fellowship program and the UIUC Support for Under-Represented Groups in Engineering (SURGE) Fellowship Program. The research was supported in part by NSF Grants CMMI No. 09-00184 ARRA and DMR No. 1106165. The PMMA microspheres that generated the nominally 10 micron diameter micropores were kindly donated by Tetsuya Okano at Sekisui Plastics Co., Ltd. (Japan).

7 References

1. Hollister SJ, Murphy WL. Scaffold translation: barriers between concept and clinic. Tissue Eng Part B Rev. 2011;17(6):459–74. [PubMed: 21902613]

2. Carragee E, Hurwitz E, Weiner B. A critical review of recombinant human bone morphogenetic protein-2 trials in spinal sugery: emerging safety concerns and lessons learned. Spine J. 2011;11(6): 471–91. [PubMed: 21729796]

3. Stoll T, Maissen O, Meury T, Becker S. New aspects in osteoinduction. Mat. -wiss. u. Werkstofftech 2004;35(4):198–202.

4. LeGeros RZ. Calcium phosphate-based osteoinductive materials. Chem Rev. 2008;108:4742–53. [PubMed: 19006399]

5. Habibovic P, Yuan H, van der Valk CM, Meijer G, van Blitterswijk CA, de Groot K. 3D microenvironment as essential element for osteoinduction by biomaterials. Biomaterials. 2005;26(17):3565–75. [PubMed: 15621247]

6. Lu J, Flautre B, Anselme K, Hardouin P, Gallur A, Descamps M, et al. Role of interconnections in porous bioceramics on bone recolonization in vitro and in vivo. J Mater Sci Mater Med. 1999;(10): 111–20. [PubMed: 15347932]

7. Hoelzle DJ, Svientek SR, Alleyne AG, Wagoner Johnson AJ. Design and manufacture of combinatorial calcium phosphate bone scaffolds. J Biomech Eng. 2011;133(10):101001. [PubMed: 22070326]

8. Hoelzle D, Alleyne A, Wagoner Johnson A. Micro-robotic deposition guidelines by a design of experiments approach to maximize process reliability for the bone scaffold application. Acta Biomater. 2008;4:897–912. [PubMed: 18378507]

9. Simon J, Michna S, Lewis JA, Rekow ED, Thompson VP, Smay JE, et al. In vivo bone response to 3D periodic hydroxyapatite scaffolds assembled by direct ink writing. J Biomed Mater Res A. 2007;83(3):747–58. [PubMed: 17559109]

10. Michna S, Wu W, Lewis JA. Concentrated hydroxyapatite inks for direct-write assembly of 3-D periodic scaffolds. Biomaterials. 2005;26(28):5632–9. [PubMed: 15878368]

11. Hing K, Annaz B, Saeed S, Revell P, Buckland T. Microporosity enhances bioactivity of synthetic bone graft substitutes. J Mater Sci Mater Med. 2005;16:467–75. [PubMed: 15875258]

12. Cordell J, Vogl M, Wagoner Johnson A. The influence of micropore size on the mechanical properties of bulk hydroxyapatite and hydroxyapatite scaffolds. J Mech Behav Biomed Mater. 2009;2(5):560–70. [PubMed: 19627863]

13. Hing KA, Best SM, Tanner KE, Bonfield W, Revell PA. Mediation of bone ingrowth in porous hydroxyapatite bone graft substitutes. J Biomater Res A. 2004;68(1):187–299.

14. Polak S, Lan Levengood S, Wheeler M, Maki A, Clark S, Wagoner Johnson A. Analysis of the roles of microporosity and BMP-2 on multiple measures of bone regeneration and healing in calcium phosphate scaffolds. Acta Biomater. 2011;7(4):1760–71. [PubMed: 21199692]

15. Lan Levengood S, Polak S, Poellmann M, Hoelzle D, Maki A, Clark S, et al. The effect of BMP-2 on micro and macroscale osteointegration of biphasic calcium phosphate scaffolds with multiscale porosity. Acta Biomater. 2010;6:3283–91. [PubMed: 20176148]

16. Lan Levengood S, Polak S, Wheeler M, Maki A, Clark S, Jamison R, et al. Multiscale osteointegration as a new paradigm for the design of calcium phosphate scaffolds for bone regeneration. Biomaterials. 2010;31:3552–63. [PubMed: 20153042]

17. Ohtsubo S, Matsuda M, Takekawa M. Angiogenesis after sintered bone implantation in rat parietal bone. Histol Histopathol. 2003;18:153–63. [PubMed: 12507295]

18. Annaz B, Hing K, Kayser M, Buckland T. Porosity variation in hydroxyapatite and osteoblast morphology: a scanning electron microscopy study. J Microscopy. 2004;215(1):100–10.

19. Habibovic P, Sees T, van den Doel M, van Blitterswijk C, de Groot K. Osteoinduction by biomaterials - physiochemcial and structural influences. J Biomed Mater Res A. 2006;77A(4): 747–62.

20. Woodard JR, Hilldore AJ, Lan SK, Park CJ, Morgan AW, Eurell JA, et al. The mechanical properties and osteoconductivity of hydroxyapatite bone scaffolds with multi-scale porosity. Biomaterials. 2007;28:45–54. [PubMed: 16963118]

21. Hing K Bioceramic bone graft substitutes: influence of porosity and chemistry. International J Appl Ceram Tech. 2005;2(3):184–99.

22. Park J. Chapter 9 Hydroxyapatite Bioceramics: properties, characterizations, and applications. Springer Verlag;

23. LeGeros R, Daculsi G, LeGeros J. Orthopedic Biology and Medicine: Musculoskeletal Tissue Regeneration In: Pietrzak W, editor. Biological Materials and Methods. Totowa, NJ: Human Press;
24. Daculsi G, Legoux F, Layrolle P. The micro macroporous biphasic calcium phosphate concerpt for bone reconstruction and tissue engineering In: Basu B, Katti D, Kumar A, editors. Advance materials: fundamentals, processing, and applications. The American Ceramic Society; 2009.
25. Mouton PR. Principles and practices of unbiased stereology: an introduction for bioscientists. Baltimore: John Hopkins University Press; 2002.
26. Alexander B, Daulton T, Genin G, Lipner J, Pasteris J, Wopenka B, et al. The nanometre-scale physiology of bone: steric modelling and scanning transmission electron microscopy of collagen-mineral structure. J Royal Soc Interface. 2012;9(73):1774–86.
27. Harkins WD, Brown FE. The determination of surface tension (free surface energy), and the weight of falling drops: The surface tension of water and benzene by the capillary height method. J Am Chem Soc. 1919;41(4):499–524.
28. Yang L, Effler JC, Kutscher BL, Sullivan SE, Robinson DN, Iglesias PA. Modeling cellular deformations using the level set formalism. BMC Systems Bio. 2008;2(68).
29. Hochmuth R, Ting-Beall H, Beaty B, Needham D, Tran-Son-Tay R. Viscosity of passive human neutrophils undergoing small deformations. Biophys J. 1993;64:1596–601. [PubMed: 8324194]
30. Hochmuth R Micropipette aspiration of living cells. J Biomech. 2000;33:15–22. [PubMed: 10609514]
31. Ting-Beall HP, Needham D, Hochmuth RM. Volume and osmotic properties of human neutrophils. Blood. 1993;81:2774–80. [PubMed: 8490184]
32. Jones WR, Ting-Beall HP, Lee GM, Kelley SS, Hochmuth RM, Guilak F. Alterations in the Young's modulus and volumetric properties of chondrocytes isolated from normal and osteoarthritic human cartilage. J Biomech. 1999;32(2):119–27. [PubMed: 10052916]
33. Furlani D, Ugurlucan M, Ong L, Bieback K, Pittermann E, Westien I, et al. Is the intravascular administration of mesenchymal stem cells safe? Mesenchymal stem cells and intravital microscopy. Microvasc Research. 2009;77:370–6.
34. Zhou Z, Chen L. Morphology expression and proliferation of human osteoblasts on bioactive glass scaffolds. Mater Sci-Poland. 2008;26(3):505–16.
35. Toma C, Wagner WR, Bowry S, Schwartz A, Villanueva F. Fate of culture-expanded mesenchymal stem cells in the microvasculature: in vivo observations of cell kinetics. Circulation Res. 2009;104:398–402. [PubMed: 19096027]
36. Hochmuth RM. Micropipette aspiration of living cells. J Biomech. 2000;33(1):15–22. [PubMed: 10609514]
37. Darling EM, Topel M, Zauscher S, Vail TP, Guilak F. Viscoelastic properties of human mesenchymally-derived stem cells and primary osteoblasts, chondrocytes, and adipocytes. J Biomech. 2008;41(2):454–64. [PubMed: 17825308]
38. Shekaran A, Garcia A. Extracellular matrix-mimetic adhesive biomaterials for bone repair. J Biomed Mater Res A. 2011;96:261–72. [PubMed: 21105174]
39. Malmstrom J, Slotte C, Adolfsson E, Norderyd O, Thomsen P. Bone response to free form-fabricated hydroxyapatite and zirconia scaffolds: a histological study in the human maxilla. Clin Oral Implants Res. 2009;20(4):379–85. [PubMed: 19298291]

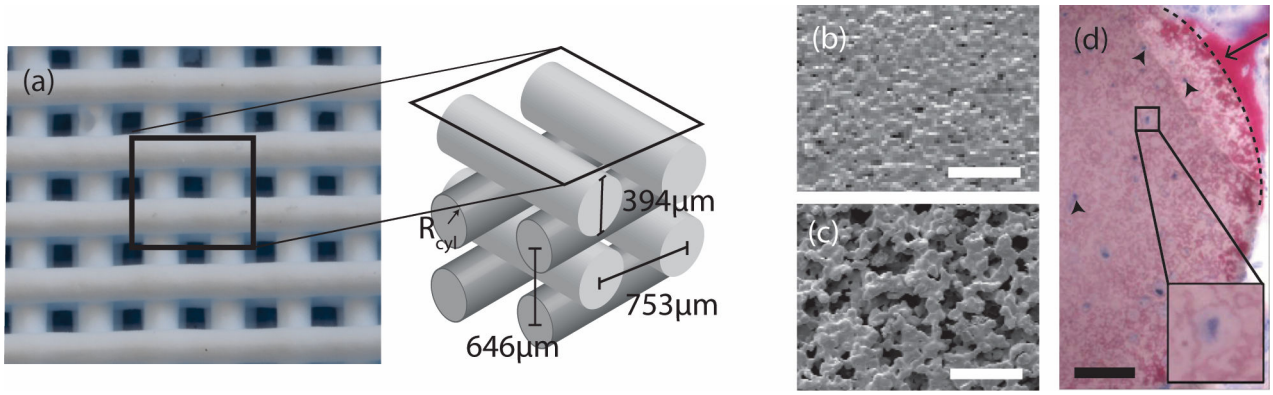

Figure 1. Characteristics of CaP scaffolds of interest.

(a) Optical image of a representative CaP scaffold lattice with orthogonal rods and a schematic of the lattice including dimensions. The rods in a given scaffold have a microstructure that is either non-microporous, NMP, **(b)** or microporous, MP **(c)**. Scale bar is 20μm. **(d)** Optical histology image showing cells in a microporous scaffold rod [15]. The image was adapted from previous work and used with permission. The sample was stained with Sanderson's rapid bone stain and counter-stained with acid fuschin. Pink/red is mineralized tissue (arrow), dark blue spots are cell nuclei (arrowheads), and the dotted line demarcates the scaffold edge. Scale bar is 50μm.

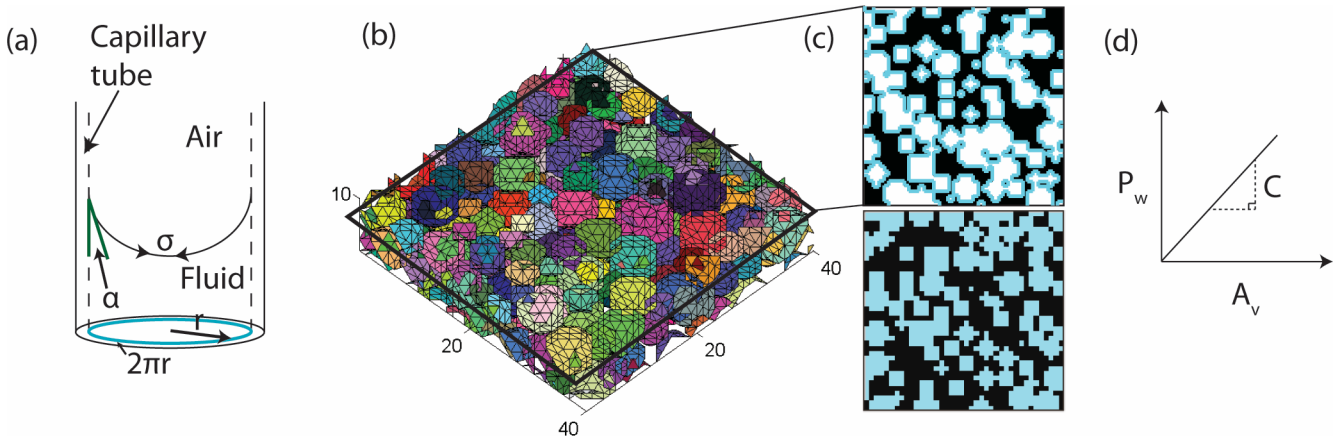

Figure 2. Capillary forces in a microporous, cylindrical rod are determined using a simulated microporous network.

(a) Schematic of capillary forces in a single capillary tube with radius r, surface tension σ, and contact angle α. The perimeter of the capillary is highlighted. **(b)** A representative volume of the simulated microstructure. Each colored sphere represents a micropore in the cylindrical rod. Units are in micrometers. Cross-sections **(c)** were taken at one-micrometer increments through the volume 10μm high for a range of cross-sectional areas, A. The top image in **(c)** highlights the wetted perimeter in blue and the bottom of **(c)** highlights the void area. **(d)** A schematic representation of the relationship between wetted perimeter, P_w, and void area, A_v, with slope C.

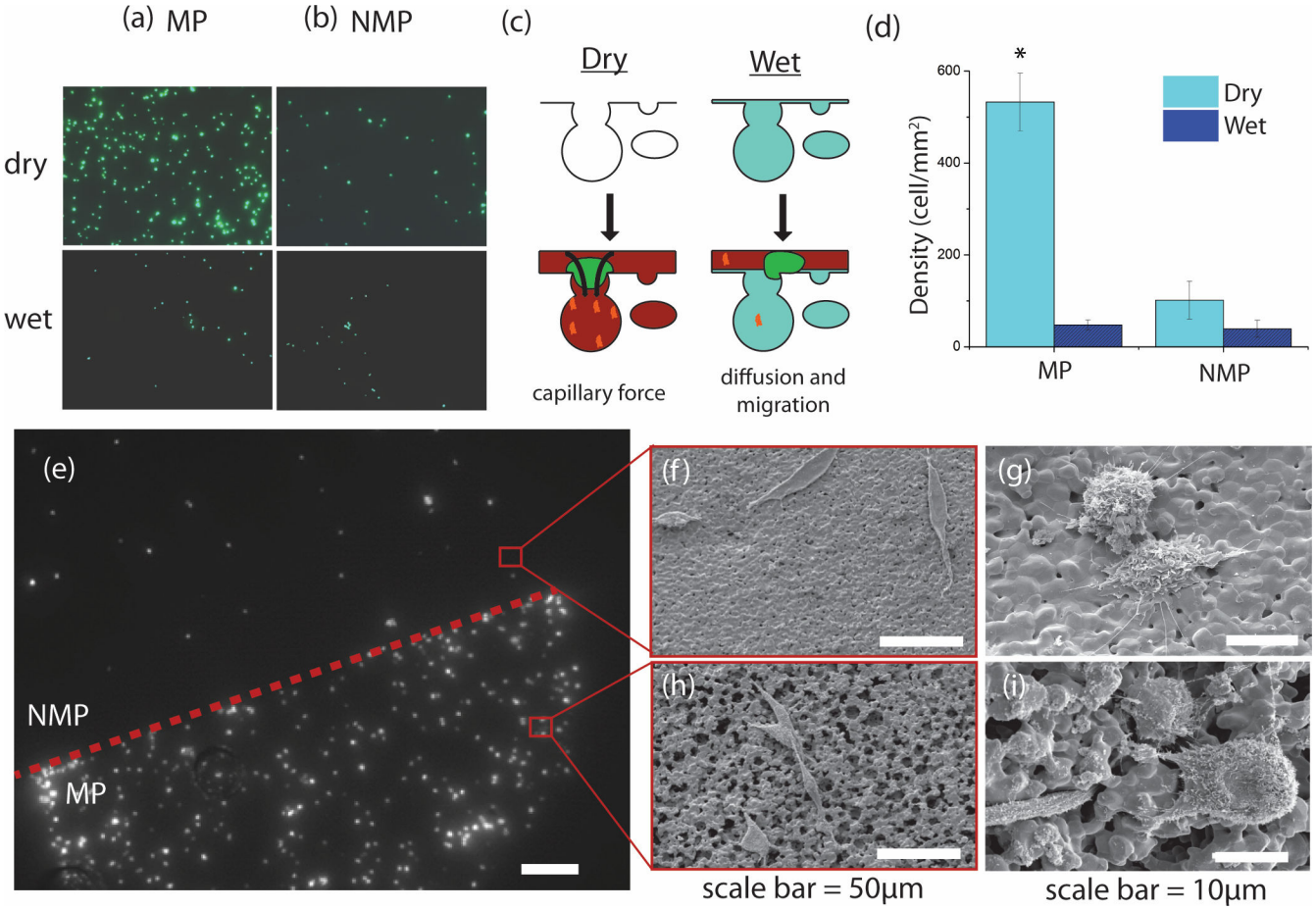

Figure 3. Capillary forces localize cells.

Column **(a)** shows the density of D1 cells on MP substrates for dry (top) and PBS-submerged (bottom) substrates. Column **(b)** shows the cell density on NMP substrates for the same cases as in **(a)**. All images are shown at 20x. **(c)** Schematic of capillary force hypothesis. Dry MP substrates will actively draw in cells and proteins in solution. MP substrates with fluid-filled pores must rely on cell migration and diffusion for cells and proteins to localize. **(d)** Dry MP substrates have a greater cell density than any of the four substrates ($p<2.5E-5$). The cell density of the dry MP substrate is eleven times that of wet MP substrate, and five times that of dry NMP substrate. There is no difference between NMP dry, NMP wet, and MP wet substrates ($p>0.05$). **(e)** Dry, composite substrate demonstrating cell localization. The upper hemi-circle is made of NMP CaP while the lower hemi-circle is made of MP CaP. Scale bar = 500µm. **(f-i)** scanning electron microscopy (SEM) images of MP and NMP substrate surfaces with D1 cells. Cells were stained with Cell-Tracker Green (CellTracker™ Green CMFDA) for fluorescent imaging.

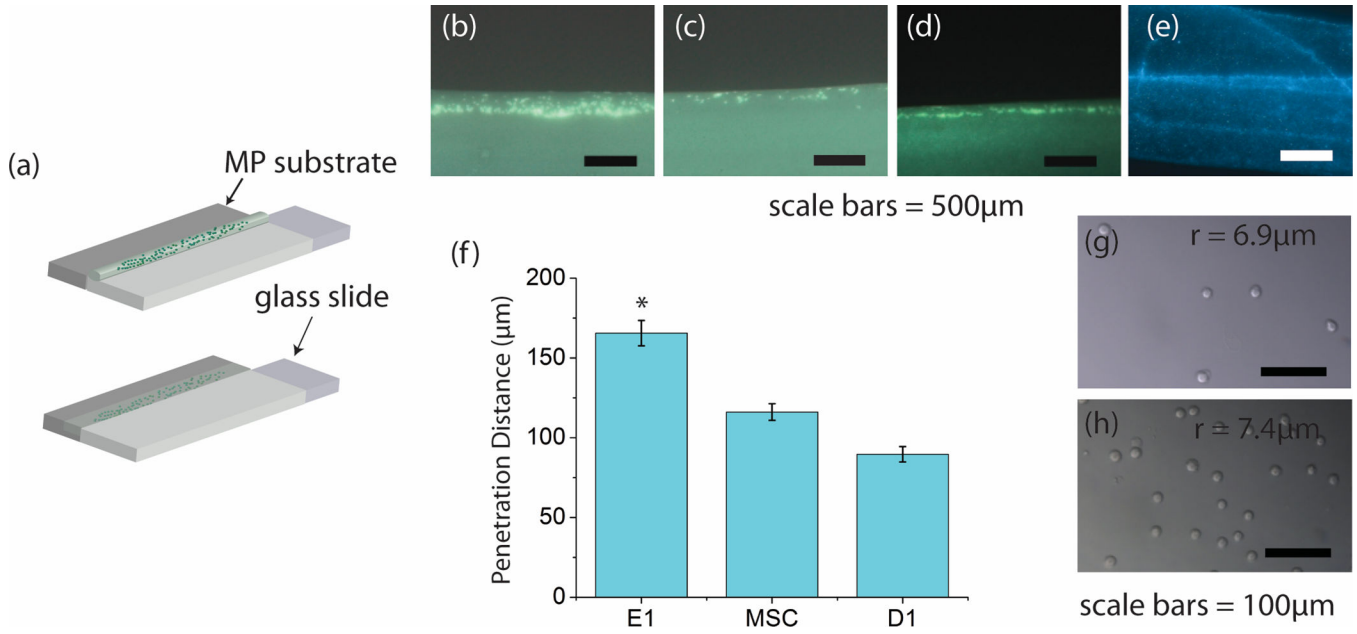

Figure 4. Capillary force experiments show cell-type penetration depth and bead penetration.

(a) Schematic representation of the experimental procedure. The substrate (dark grey) was brought into contact with the solution containing either cells or hard beads on the edge of the slide. This resulted in bead/cell motion due only to capillary forces. **(b)**, **(c)**, and **(d)** are representative images of E1, MSC, and D1 cell penetration, respectively. **(e)** Fluorescent image of the substrate after contact with the bead solution. The edge of the substrate that contacted the coverslip is at the bottom of the image. The dark region directly above the region containing the fluorescent beads is the remainder of the substrate through which the beads did not penetrate. **(f)** Average measured distance traveled by each cell type. The E1 cells penetrate significantly further than the MSCs and D1s ($p<5E-5$). E1s **(g)** and D1s **(h)** in solution imaged using bright field microscopy. E1s have a radius of 6.9 ± 0.65μm and the D1s have a radius of 7.5 ± 1.20μm.

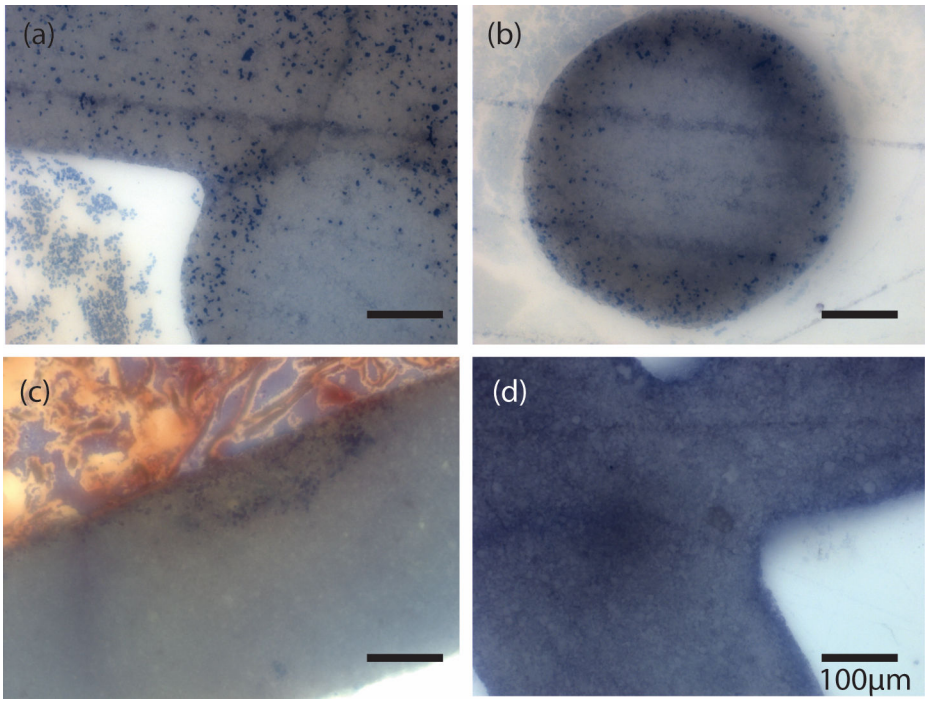

Figure 5. Histologic images of MP scaffolds implanted in porcine mandibular defect for 30 minutes.

(a) and (b) are MP scaffolds implanted dry. (c) and (d) are MP scaffolds implanted after submerging in saline, which filled micropores with solution. All images are stained with Sanderson's rapid bone stain. Dark blue = cell nuclei.

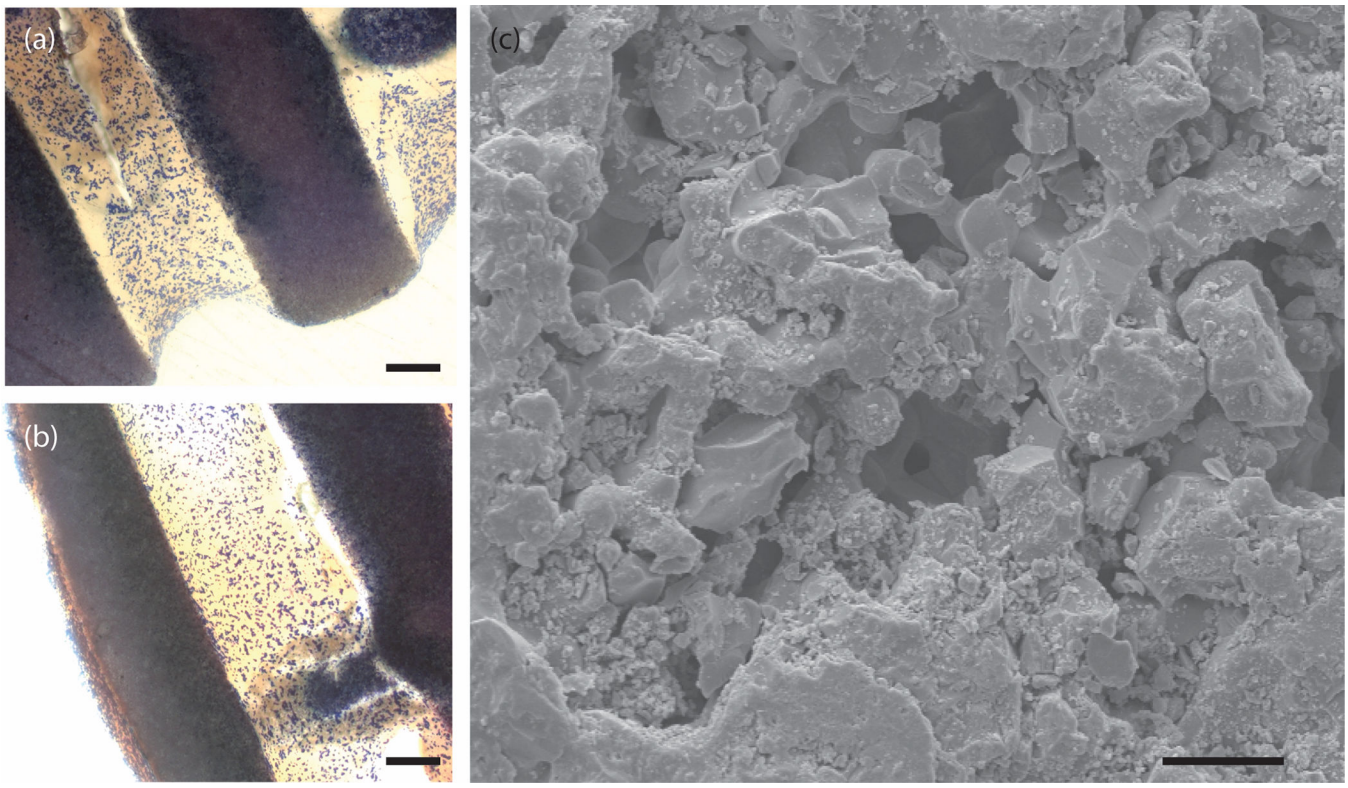

Figure 6. Edge effects in capillary forces.

(a) and (b) are histologic images of 30 minute implanted dry MP scaffolds. The stain is Sanderson's rapid bone stain which colors cell nulcei dark blue. Note the end-milled areas such as the lower portions of the rods in (a) and the side portion of the rod in (b) lack cells. Scale bars = 100μm. (c) is an SEM image of the end-milled face of an MP scaffold. Note the debris in the micropores. Scale bar = 5μm.

Table 1.

Critical pressure for a cell to enter a single capillary and cell penetration distances in microporous substrates.

Critical pressures required for different cell types to enter a pore with a radius of 2.5μm. Neutrophils require the least pressure, while chondrocytes require the most. Penetration distance determined experimentally for three cell types used in this study is given. E1s penetrate the greatest distance and the difference was statistically significant ($p<0.001$). Data obtained from the literature are indicated by the adjacent reference. Other values were not available (N/A) or were measured experimentally.

Cell	γ_{ten} (kg/s^2)	R_c (μm)	P_{crit} (Pa)	Distance (μm)
Neutrophil	0.000024 [29]	4.2 [31]	7.77	N/A
Osteoblast	0.00052 *	7.5 [34]	277	N/A
MSC	0.00052 [35]	11.5 [33,35]	326	116
Chondrocyte	0.0022 [30]	7.0 [32]	1131	N/A
D1	N/A	7.5	N/A	89.6
E1	0.00052 **	6.9	265	165

* The cortical tension for MSCs was used for osteoblasts, however the osteoblast cortical tension is less than the MSC cortical tension due to the osteoblast's similar elastic modulus [37] but smaller radii [30,33,34]

** The cortical tension for osteoblasts was used for the E1 cells.